Atom-interferometric measurement of Stark level splittings

Limei Wang, Hao Zhang, Linjie Zhang, Georg Raithel, Jianming Zhao, and Suotang Jia

Phys. Rev. A **92**, 033619 — Published 21 September 2015

DOI: 10.1103/PhysRevA.92.033619

Atom-interferometric measurement of Stark level splittings

Limei Wang, Hao Zhang, Linjie Zhang, Georg Raithel[1], Jianming Zhao,* and Suotang Jia
State Key Laboratory of Quantum Optics and Quantum Optics Devices,
Institute of Laser spectroscopy, Shanxi University, Taiyuan 030006, P. R. China and
[1]*Department of Physics, University of Michigan, Ann Arbor, Michigan 48109-1120, USA*

Adiabatic/diabatic passages through avoided crossings in the Stark map of cesium Rydberg atoms are employed as beam splitters and recombiners in an atom-interferometric measurement of energy-level splittings. We subject cold cesium atoms to laser-excitation, electric-field and detection sequences that constitute an (internal-state) atom interferometer. The adiabatic state transformation in the interferometer's beam splitters enables the spectroscopy of states that are, due to selection rules, inaccessible to direct laser-spectroscopic observation. For the read-out of the interferometer we utilize state-dependent collisions, which selectively remove atoms of one kind from the detected signal. We investigate the dependence of the interferometric signal on timing and field parameters, and find good agreement with quantum simulations of the interferometer. Fourier analysis of the interferometric signals yield coherence frequencies that agree with corresponding energy-level differences in calculated Stark maps.

PACS numbers: 37.25.+k, 32.80.Xx, 32.80.Ee
Keywords: atom interferometry, level crossings, Rydberg state

I. INTRODUCTION

Matter-wave interference offers exquisite sensitivity to measure fields and atomic or molecular interactions. Examples based on atom inertia include atom-interferometric gravimetry [1–3], gradiometry [4, 5], and Sagnac-type rotation sensors (gyroscopes) [6, 7]. Such devices usually involve laser-based beam splitters to coherently split and recombine wavefunctions. Another well-known example of matter-wave interference is the superconducting quantum interference device (SQUID) [8], which engages the vector potential to measure magnetic-field-induced phases [9–11]. Applications of Ramsey's separated-oscillatory-field method [12], which employs quantum interference between field-coupled internal states of a quantum particle, are abound in spectroscopy and time metrology [13, 14]. In the Sokolov atom interferometer, a rectangular electric-field pulse couples the $2S_{1/2}$ and $2P_{1/2}$ states of hydrogen into and out of two mixed Stark states, and the interferometric signal is observed via the Lyman-α fluorescence from $2P_{1/2}$ [15, 16].

Interferometric methods also extend to Rydberg atoms. These highly excited atoms are attractive in field metrology due to their strong response to applied electric fields (polarizabilities typically scale $\propto n^7$[17]) and microwave/THz fields. Couplings between Floquet states of thermal Rydberg atoms in microwave fields give rise to Stückelberg oscillations [18] and interference effects in microwave multiphoton excitation [19, 20]. Stückelberg oscillations based on avoided crossings between two-atom energy levels shifted by the dipole-dipole interaction between Rydberg atoms have been investigated in an oscillating radio-frequency field [21]. Ramsey interferometry involving optical and external-electric-field pulses has been employed to detect Stark-tuned Förster resonances and the interaction-induced phase shift of cold rubidium Rydberg atoms [22, 23].

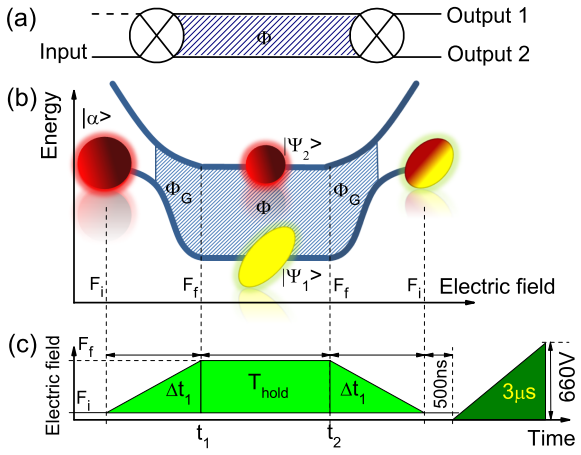

FIG. 1: (color online) (a) Schematic principle of the atom interferometer. (b) Atom interference of $nS_{1/2}$ and high-l Stark Rydberg states through an electric-field-induced avoided crossing. After preparing a Rydberg Stark state $|\alpha\rangle$ at an initial field F_i, the field is ramped to a variable final field F_f. During the ramp time through the crossing, Δt_1, the atoms undergo mixed diabatic/adiabatic passage into adiabatic states $|\Psi_1\rangle$ and $|\Psi_2\rangle$, respectively. After a variable hold time $T_{\rm hold} < 60$ ns, the electric field is ramped back to F_i. (c) Timing of the ramped electric field (light green) and the state-selective ionization field (dark green) used to read out the interferometer. Collisions during the waiting time of 500 ns before the rise of the ionization field enable state-selective detection (see text).

In internal-state atom interferometers, input and out-

*Corresponding author: zhaojm@sxu.edu.cn

put states are coherently mixed and recombined into and out from superposition states that exist between mixing and recombination [see Fig. 1 (a)]. The interference pattern arises from the accumulated interferometric phase Φ (hatched areas in Fig. 1) and is observed as a population difference at the output. Note the analogy with optical Mach-Zehnder interferometers. In our Rydberg-atom interferometer, avoided crossings in the Stark map are utilized as beam splitters and recombiners. The coherent state mixing occurs during multiple passages of the atoms through the avoided crossings. A time-dependent electric field acts as a control parameter for the passage behavior. In the return passage, the accumulated phase of the wavefunction coherence is mapped into a measurable population difference between the adiabatic Rydberg states of the system. Using the sequence displayed in Fig. 1 (b) and (c), we study the dependence of the interferometric response on the inside electric field, F_f, the ramp time, Δt_1, and the electric-field hold time between the ramps, $T_{\rm hold}$. The coherence frequencies, obtained by Fast Fourier Transforms (FFTs) of the interferometric signals, are compared with a theoretical model. We note that the interferometer described in this work is a quantum interferometer acting on the internal states of the atoms, while the center-of-mass wavefunction remains unaffected.

From the viewpoint of Rydberg-atom spectroscopy, the internal-state interferometer demonstrated in our work presents a non-optical means to study energy levels that are inaccessible to laser excitation. In our case, linear Stark states accessed via the interferometer's beam splitters (the avoided crossings) cannot be optically excited because of their small oscillator strengths with the lower atomic state used in the laser excitation. The state transformation associated with adiabatic passage through the avoided crossings enables the population of these hidden states. Measurement of the phase $\Phi(T_{\rm hold})$ in Fig. 1 yields information on the energies of the hidden states that become populated within the interferometer.

II. EXPERIMENTAL METHOD

The cesium atoms are trapped in a standard magneto-optical trap; for details see Ref. [24]. As shown in Fig. 2, the Rydberg atoms are initially prepared in the well-defined adiabatic state $|\alpha\rangle$, in the initial electric field F_i. When the electric field is ramped to its final value F_f, mixed diabatic/adiabatic passage through the selected avoided crossing coherently splits the wavefunction into the adiabatic states $|\Psi_2\rangle$, which predominantly has $49S_{1/2}$-character, and $|\Psi_1\rangle$, which is a hydrogen-like linear Stark state with predominantly high-l character.

The selected avoided crossing is centered at $F_X = 3.19$ V/cm (dotted circle in Fig. 2). After the holding time $T_{\rm hold}$ at F_f, the electric field is ramped back to F_i. The atoms pass the selected avoided crossing twice, namely at times near t_1 and t_2. The differential phase Φ

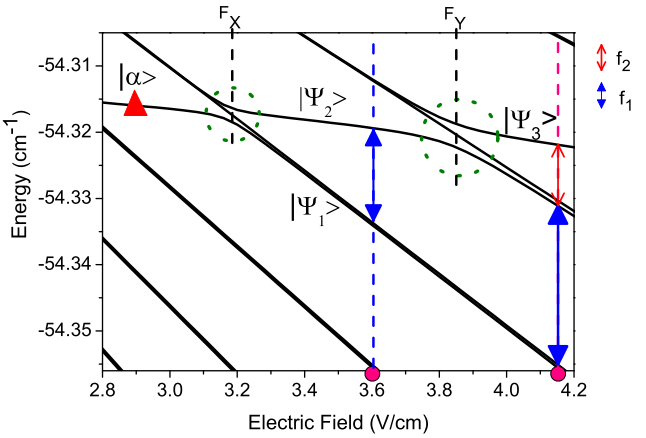

FIG. 2: (color online) Calculated Stark map in the vicinity of the $49S_{1/2}$ state and the n=45 manifold of cesium over the field range 2.8-4.2 V/cm. The range covers two avoided crossings centered at $F_X = 3.19$ V/cm and $F_Y = 3.85$ V/cm, respectively. We study the regions $F_X < F_f < F_Y$ and $F_f > F_Y$ (corresponding to the dots on the field axis). In both regions the interferometric signal contains the coherence frequency f_1 (blue wide arrow), which originates in coherent splitting and recombination at field F_X. The interferometric signal in the second region exhibits additional frequencies f_2 (red thin arrow) and f_1+f_2, which arise due to additional splitting and recombination at field F_Y.

between $|\Psi_1\rangle$ and $|\Psi_2\rangle$ accumulated between t_1 and t_2 is given by

$$\Phi(T_{\rm hold}) = \Phi_G + \frac{1}{\hbar}\int_{t_1}^{t_2=t_1+T_{\rm hold}} (E_2 - E_1)dt \quad , \qquad (1)$$

where Φ_G includes a geometrical phase that depends on the passage through the crossing. The integral reflects the dynamical phase accumulated during the hold time. The energy difference $E_2 - E_1$ between $|\Psi_2\rangle$ and $|\Psi_1\rangle$ at the final field is approximately given by $E_2 - E_1 = -\Delta d(F_f - F_X)$, where Δd is the difference between the electric-dipole moments of $|\Psi_2\rangle$ and $|\Psi_1\rangle$ at field F_f. For fixed Δt_1 the interferometric phase then is

$$\Phi(T_{\rm hold}) \approx \Phi_G - \frac{1}{\hbar}\Delta d(F_f - F_X)T_{\rm hold} \quad , \qquad (2)$$

i.e. it accumulates at a rate given by the final field F_f. Each time the field passes through F_X, the adiabatic states $|\Psi_1\rangle$ and $|\Psi_2\rangle$ are subject to coherent mixing. We detect the fraction of the atom population that exits the interferometer in the original S-like state $|\alpha\rangle$. Experimentally, the 500 ns waiting period before detection is critical because it enables state-selective readout by separating the elongated high-l Stark state and state $|\alpha\rangle$ through m-mixing collisions [25]. The collisions render most atoms in high-l states undetectable due to an increase in field ionization voltage beyond 660 V (see Fig. 1).

III. THEORETICAL MODEL

To model our experiment, we numerically obtain the Stark energy level structure for cesium and simulate the time evolution of the wavefunction. To obtain the time-independent Stark energy level structure, we use methods described in [26] and quantum defects from [17]. Figure 2 shows the relevant range of the cesium Stark structure. The $49S_{1/2}$-like level encounters two avoided crossings centered at F_X and F_Y, which have energy gaps of 58 MHz and 110 MHz, respectively. Rydberg atoms initialized in state $|\alpha\rangle$ are propagated into final state $|\Psi_{\rm end}\rangle$ by integrating the time-dependent Schrödinger equation for the sequence in Fig. 1 with Hamiltonian:

$$\hat{H} = \frac{\hat{\mathbf{p}}^2}{2\mu} - \frac{1}{\hat{r}} + V_c(\hat{r}) + V_{FS} + F(t)\hat{z} \quad , \qquad (3)$$

here V_c is a short-range core potential, V_{FS} is the fine structure, and $F(t)\hat{z}$ is the perturbation due to the time-dependent electric field. The interferometric signal $S = |\langle\alpha|\Psi_{\rm end}\rangle|^2$, *i.e.* the probability of returning to the initially excited S-like Stark state, is computed as function of hold time $T_{\rm hold}$, ramp time Δt_1, and field F_f.

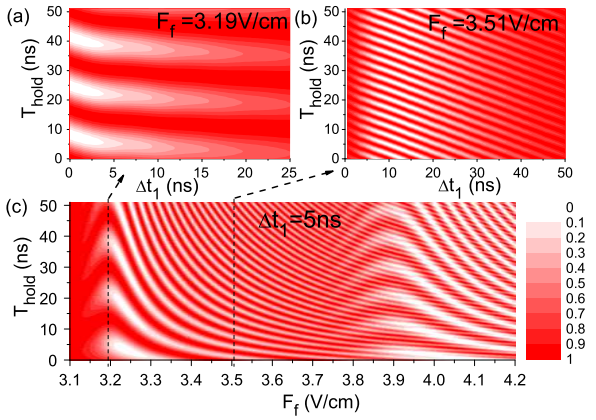

FIG. 3: (color online) (a) Interferometric signal S versus ramp duration Δt_1 and holding time $T_{\rm hold}$ when ramping the electric field from F_i=2.9 V/cm to $F_f = F_X = 3.19$ V/cm (the center field of the first avoided crossing in Fig. 2). (b) Same as (a), but for $F_f = 3.51$ V/cm (between the two crossings in Fig. 2). (c) Signal S versus $T_{\rm hold}$ and final field F_f, for fixed $F_i = 2.9$ V/cm and $\Delta t_1 = 5$ ns.

In Fig. 3 (a) we set $F_f = F_X$ and show the signal $S(T_{\rm hold})$ versus Δt_1. The signal $S(T_{\rm hold})$ oscillates with a period of 17 ns, corresponding to the gap of 58 MHz between levels $|\Psi_1\rangle$ and $|\Psi_2\rangle$ at the first avoided crossing [27]. The visibility of the oscillation is maximal for $\Delta t_1 = 0$, because sudden projection of the initial state $|\alpha\rangle$ into the center field F_X of the crossing yields amplitudes near $1/\sqrt{2}$ for both coupled levels. As Δt_1 increases, the evolution becomes increasingly adiabatic, and the splitting ratio continuously changes from 50% to 100% adiabatic. Hence, as seen in Fig. 3 (a), the visibility of the oscillation in S diminishes with increasing Δt_1.

In Fig. 3 (b) the field $F_f = 3.51$ V/cm, which is in-between two avoided crossings. As before, the oscillation frequency of S is given by the energy difference between the adiabatic states $|\Psi_2\rangle$ and $|\Psi_1\rangle$, but the visibility of the oscillation in the signal S peaks at $\Delta t_1 = 16$ ns. In this case, the interference signal peaks under conditions when the Landau-Zener passage dynamics through the crossing leads to 50% population in each of the adiabatic states $|\Psi_2\rangle$ and $|\Psi_1\rangle$. A straightforward calculation for a two-level Landau-Zener crossing with gaps and slopes as in Fig. 2 shows that parity between diabatic and adiabatic passage probability is indeed expected at $\Delta t_1 = 16$ ns [27].

The phase shift of the modulations in $S(T_{\rm hold})$ seen when varying Δt_1 or F_f reflects a variation of Φ_G in Eq. 2, which arises from the phases that occur during the splitting and recombination of the atomic state. Since Φ_G does not affect the frequency of the interferometric signal observed when varying $T_{\rm hold}$, the phase Φ_G does not affect the atomic level splitting(s) deduced from the frequency component(s) contained in $S(T_{\rm hold})$. The phase Φ_G also does not affect the visibility of the interference signal, which only depends on the moduli of the amplitudes that occur during the splitting and recombination.

For our experimental studies, presented in Sec. IV, a choice of $\Delta t_1 = 5$ ns yields high interference contrast in $S(T_{\rm hold})$ for all values of F_f. In Fig. 3 (c) we plot $S(T_{\rm hold})$ as a function of the final electric field F_f for a fixed $\Delta t_1 = 5$ ns. Interferometric oscillations in S are clearly visible over a wide range F_f, with frequencies that reflect the energy splittings in the Stark map. The oscillation frequency increases with F_f in the domain $F_X \lesssim F_f \lesssim F_Y$; this frequency corresponds to f_1 (blue wide arrow in Fig. 2). When the final field is increased beyond F_Y, the signal $S(T_{\rm hold})$ displays several frequencies. Noting that mixed diabatic/adiabatic passage from $F_i = 2.9$ V/cm to $F_f \gtrsim F_Y$ will generate amplitudes in all three adiabatic states $|\Psi_1\rangle$ to $|\Psi_3\rangle$ in Fig. 2, we expect to find three frequencies in that domain, f_1, f_2 (red thin arrow), and their sum $f_1 + f_2$.

IV. EXPERIMENTAL DATA

In Fig. 4 we show experimental interferometric signals $S(T_{\rm hold})$ for $F_f = 3.60$ V/cm [panel (a), left plot] and $F_f = 4.15$ V/cm [panel (b), left plot]. The plots on the right show the respective spectral powers of FFTs of the measured $S(T_{\rm hold})$. To suppress artifacts at low frequencies and spectral side lobes, we subtract the time-averaged values of S and multiply with a standard window function (the Hanning window) before computing the FFTs. The experimental data were sampled in 1 ns steps, the smallest step size of the waveform generator used to generate the time-dependent electric field.

The peaks in experimental Fig. 4 at 438 MHz for 3.60 V/cm and 297 MHz for 4.15 V/cm are in good agreement with the Stark-map frequencies labeled f_1 and f_2 in

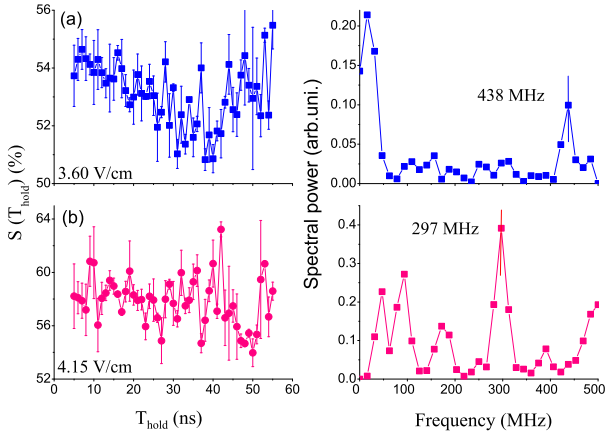

FIG. 4: (Color online) Interferometric signal S versus $T_{\rm hold}$ (left panels) and powers of the corresponding FFTs (right panels) for two values of the final electric field, F_f = 3.60 V/cm (a) and 4.15 V/cm (b).

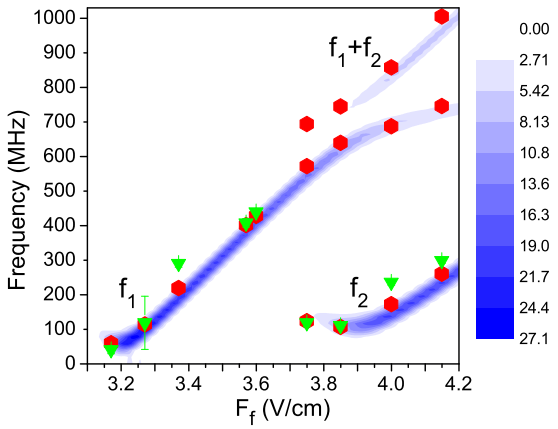

FIG. 5: (Color online) Measured coherence frequencies (green triangles) and corresponding calculated frequency differences f_1, f_2, and f_1+f_2 between Stark states (red diamonds) vs. the final electric field, F_f. The gray-scale plot in the background shows the FFT spectral density obtained from Fig. 3 (c).

Fig. 2, respectively. The peak near 20 MHz in Fig. 4 (a) is discarded because it appears to reflect an overall, slow signal drift that occurred while taking the signal $S(T_{\rm hold})$.

In Fig. 4 (a) we show a coherence via mixed diabatic/adiabatic passage through the crossing at field F_X in Fig. 2, and the coherence evolves at a frequency given by the Stark splitting between adiabatic states $|\Psi_2\rangle$ and $|\Psi_1\rangle$ at F_f =3.60 V/cm. Our interferometric measurement allows us to measure frequency splittings involving states that are optically not excitable due to selection rules. In the instance of Fig. 4 (a), the linear Stark state $|\Psi_1\rangle$ at 3.60 V/cm has a weak oscillator strength with low-lying S and P-levels. Adiabatic passage through the avoided crossing at field F_X into the optically non-excitable state $|\Psi_1\rangle$ serves as a way to circumvent optical selection rules: it allows us to probe a state that is hidden in the optical excitation spectrum.

In Fig. 4 (b) the ramp speed is faster due to larger F_f and constant Δt_1, and the passage through the first crossing is mostly diabatic. The passage through the second crossing (F_Y in Fig. 2) leads to an adiabatic/diabatic splitting ratio near 50%/50%, which results in a signal in which the frequency component f_2 between levels $|\Psi_3\rangle$ and $|\Psi_2\rangle$ has a high amplitude (*i.e.* the corresponding oscillation in the interferometric signal $S(T_{\rm hold})$ has a high visibility). Fig. 4 (b) therefore shows that our interferometric method offers flexibility in measuring energy-level differences involving a variety of hidden states of interest. This is done by selecting specific avoided crossings and ramp speeds that result in significant populations in the optically unaccessible states of interest.

We have performed a series of additional measurements $S(T_{\rm hold})$ for different final fields F_f and calculated their FFTs (Fig. 5, green triangles). The experimental frequencies are compared with corresponding frequency spacings f_1, f_2, and $f_1 + f_2$ calculated from the Stark map in Fig. 2 (red diamonds). The backdrop shows the FFT of the simulated signals from Fig. 3 (c). The simulated FFTs show signals up to 1 GHz (the simulation has a sampling step size of 0.2 ns and a Nyquist frequency of 2.5 GHz; between 1 GHz and 2.5 GHz the simulated FFTs do not show significant signals). All three types of data in Fig. 5 are consistent with each other. It is noted that only f_1, f_2 and $f_1 + f_2$ significantly contribute to the FFTs of the interferometric signal, despite the fact that hundreds of Stark states near the selected avoided crossings are included in the calculation. According to the interpretation given above, this is due to the fact that only the adiabatic levels $|\Psi_1\rangle$, $|\Psi_2\rangle$ and $|\Psi_3\rangle$ become populated due to coupling at the selected avoided crossings. Notably, the splittings measured away from the level crossings involve elongated high-l Stark states that are, due to a lack of oscillator strength, not observed in laser-spectroscopic Stark maps.

V. DISCUSSION

Since we scan the hold time $T_{\rm hold}$ over a range of 60 ns, our basic Fourier resolution limit is $\gtrsim$ 15 MHz. Moderate additional broadening by a factor $\lesssim 2$ occurs due to the utilized FFT window. In the following we briefly discuss how the resolution could be improved in the future.

To reduce the linewidth in measurements such as in Fig. 5, one may increase the $T_{\rm hold}$ scan range until it reaches the intrinsic coherence time $T_{\rm coh}$ of the interferometer, where inhomogeneous phase variations approach $\delta\Phi \sim \pi$. The value of $T_{\rm coh}$ is limited mostly by temporal and spatial variations in the electric field, and to a lesser degree by Rydberg-atom collision times and radiative decay times. The value of $T_{\rm coh}$, the field variation δF and the dipole-moment difference Δd satisfy $\Delta d\, T_{\rm coh}\, \delta F \lesssim \pi\hbar$. In the present case ($T_{\rm hold}$ scan range 60 ns and $\Delta d \approx 700$ ea$_0$) the requirement on the field inhomogeneity is $\delta F \lesssim 10$ mV/cm. This amounts to about

0.3% of the maximal applied field F_f, or about 1% of the maximal electric-field differential $F_f - F_X$ (the quantity relevant in Eq. 2). In the present setup, the diameter of the excitation volume (~ 50 μm) is several orders of magnitude smaller than the separation between the parallel grids used to generate the field (15 mm), and the excitation volume is centered relative to the grids [25]. Therefore, the spatial variation of the field is estimated to be well below the above limits. We expect that future increases of the coherence time will mostly result from improvements in the temporal stability of the field.

In conclusion, we have observed the coherence between quantum states using an interferometric method in which an external electric field is ramped twice through selected avoided crossings in the Cs Stark map. The interferometric signal is observed by varying the hold time between the field ramps. The coherence frequencies observed in the Fourier transforms of the signal reflect the energy-level differences in the underlying Stark map. The method allows us to map out levels that, due to selection rules, are hidden in optical excitation spectra. Future work may include the study and improvement of the coherence time of the interferometer, as well as measurements of level shifts of hidden Stark states due to DC and AC-fields and collisions.

The work was supported by the 973 Program (2012CB921603), the NSFC Project for Excellent Research Team (61121064), the NNSF of China (11274209, 61475090, 61378039 and 61378013) and the NSF (PHY-1205559).

[1] M. de Angelis, A. Bertoldi, L. Cacciapuoti, A. Giorgini, G. Lamporesi, M. Prevedelli, G. Saccorotti, F. Sorrentino, and G M Tino, Meas. Sci. Technol. **20**, 022001 (2009).
[2] K. J. Hughes, J. H. T. Burke, and C. A. Sackett, Phys. Rev. Lett. **102**, 150403 (2009).
[3] R. Geiger, V. Ménoret, G. Stern, N. Zahzam, P. Cheinet, B. Battelier, A. Villing, F. Moron, M. Lours, Y. Bidel, A. Bresson, A. Landragin, and P. Bouyer, Nat. Commun. **2**, 474 (2011).
[4] J. M. McGuirk, G. T. Foster, J. B. Fixler, M. J. Snadden, and M. A. Kasevich, Phys. Rev. A **65**, 033608 (2002).
[5] N. Yu, J. M. Kohel, J. R. Kellogg, and L. Maleki, Appl. Phys. B **84**, 647 (2006).
[6] T. L. Gustavson, A. Landragin, and M. A. Kasevich, Class. Quantum Grav. **17**, 2385 (2000).
[7] A. Lenef, T.D. Hammond, E.T. Smith, M.S.Chapman, R.A. Rubenstein, D.E.Pritchard, Phys. Rev. Lett. **7**8, 760 (1997).
[8] R L Fagaly, Rev. Sci. Instrum. **77**, 101101 (2006).
[9] R. K. Varma, S. B. Banerjee, and A. Ambastha, Eur. Phys. J. D **66**, 38(2012).
[10] R. K. Varma, Phys. Rev. E, **64**, 036608 (2001).
[11] R. K. Varma, A. M. Punithavelu, and S. B. Banerjee, Phys. Rev. E **65**, 026503 (2002).
[12] N. F. Ramsey, Rev. Mod. Phys. **62**, 541 (1990).
[13] A. D. Cronin, J. Schmiedmayer and D. E. Pritchard, Rev. Mod. Phys. **81**, 1051 (2009).
[14] K. Hornberger, S. Gerlich, P. Haslinger, S. Nimmrichter, and M. Arndt Rev. Mod. Phys. **84**, 157 (2012).
[15] Yu. L. Sokolov, **The hydrogen atom**, Proc. Symp. (Pisa, Italy, 30 June - 2 July 1988)ed G. F. Bassani, M. Inguscio and T. W. Hänsch (Berlin: Springer) (1989).
[16] J. Baudon, R. Mathevet and J. Robert, J. Phys. B: At. Mol. Opt. Phys. **32** R173 (1999).
[17] T. Gallagher, **Rydberg atoms**, Cambridge University Press, Cambridge, U.K. (1994).
[18] E. C. G. Stückelberg, Helv. Phys. Acta **5**, 369 (1932).
[19] M. C. Baruch and T. F. Gallagher, Phys. Rev. Lett. **68**, 3515 (1992).
[20] S. Yoakum, L. Sirko and P. M. Koch, Phys. Rev. Lett. **69**, 1919 (1992).
[21] C. S. E. van Ditzhuijzen, Atreju Tauschinsky, and H. B. van Linden van den Heuvell, Phys. Rev. A **80**, 063407 (2009).
[22] J. Nipper, J. B. Balewski, A. T. Krupp, B. Butscher, R. Löw, and T. Pfau, Phys. Rev. Lett. **108**, 113001 (2012).
[23] J. Nipper, J. B. Balewski, A. T. Krupp, S. Hofferberth, R. Low, and T. Pfau, Phys. Rev. X **2**, 031011 (2012).
[24] H. Zhang, L. Wang, L. Zhang, C. Li, L. Xiao, J. Zhao, S. Jia, P. Cheinet, D. Comparat, and P. Pillet, Phys. Rev. A **87**, 033405 (2013).
[25] L. Wang, H. Zhang, L. Zhang, C. Li, Y. Yang, J. Zhao, G. Raithel, and S. Jia, New J. Phys. **17**, 063011 (2015).
[26] M. L. Zimmerman, M. G. Littman, M. M. Kash, and D. Kleppner, Phys. Rev. A **20**, 2251 (1979).
[27] The state cutting through the center of the avoided crossing can be largely ignored, as found in Ref. [25].